Pressure induced structural phase transition and influence of pressure on the electronic and mechanical properties of TiPdSn: an ab initio study

M. I. Babalola^{a*}, Omamoke O. E. Enaroseha^b

^a Department of Physics, University of Benin, Nigeria.
^b Department of Physics, Delta State University Abraka, Nigeria.

E-mail: michael.babalola@uniben.edu

Abstract

Structural, electronic, mechanical and optical properties of half-Heusler alloy TiPdSn were investigated from first-principles calculation as well as the structural phase transition under pressure. The projected augmented wave (PAW) type of pseudopotential within the generalized gradient approximation (GGA) was used during the calculation. The obtained results revealed that TiPdSn is a semiconductor with an indirect band gap. Also the results from the mechanical property showed that TiPdSn is ductile and mechanically stable. TiPdSn is seen to undergo structural phase transition from cubic to two different structures namely type1 and type2 which crystallize in hexagonal structure and the transition pressures recorded were 4.53GPa for type 1 and 25.3 GPa for type 2. Optical properties revealed that TiPdSn has a static dielectric function of 21.47 and a refractive index of 4.63. The band gap of the alloy decreases and later increases as pressure increases.

Keywords: Half Heusler; Phase transition; dielectic function; Semiconductor; Bulk modulus; Band gap

1. Introduction

Half-Heusler alloys have been given much attention by researchers over the years because of their numerous properties that find application in the technological industries[1-4]. Half-Heusler alloys belong to the family of Heusler alloys which include full-Heusler alloys, quaterary Heusler alloys, half-Heusler alloys and binary Heusler alloys. The full-Heusler alloys are ususally represented by a formula X2YZ while the half-Heusler alloys are represented by a formula XYZ. The numerous properties that these alloys exhibits make them very useful as semiconductors[5], thermoelectric materials[1], superconductors[6], topological insulators[7], magnetooptical devices[8], half-metals[9], shape memory alloys[10], and as materials with heavy-Fermion behaviour[11]. Because of their very small lattice mismatch, half-Heusler alloys can be epitaxially grown on semiconductors which is used as spin injection devices[12].

The beauty of the Heusler alloy family is that their properties can be predicted just by knowing the number of valence electrons. For instance, half-Heusler alloys with valence electrons of 18 are known to possess semiconducting property[13] as well as thermoelectric property[14]. Half-Heusler alloys with valencies less than or greater than 18 are usually ferromagnetic with some of them possesing the half-metallic properties[15]. TiPdsn is an example of 18 valence electron with semiconducting

behaviour and several of its properties have been investigated. Kaur (2017) investigated the electronic, lattice dynamics and thermoelectric properties of TiPdSn[16]. He observed that TiPdSn is an indirect band gap semiconductor. Dasmahapatra et al. studied the electronic, mechanical and thermoelectric properties of TiPdSn and noted that TiPdSn has a figure-of-merit of approximately 1[17]. Zheng et al. also investigated how the thermoelectric property of TiPdSn is influenced when doped with Zr[18]. They found out that Ti0.5Zr0.5PdSn had a high figure of merit of 2.43. Gautier and his colleagues investigated a number of 18 valence electron half-Heusler alloys and found out that TiPdSn is a stable half-Heusler alloy[19].

The optical property of TiPdSn is scarce in literature and the need to know the behaviour of TiPdSn with light is very invaluable in opto-electronic field. Half-Heusler alloys also crystallize in hexagonal crystal struture with space group P63/mmc No. 194 and P63 mc No. 186. Structural phase transition from cubic phase to hexagonal phase under pressure has been reported experimentally[20] and theoretically[21] by researchers. In this study, investigation is carried out on the structural phase transition of TiPdSn from cubic phase to hexagonal phases under pressure. The optical property was also investigated. The influence of pressure was also carried out on the electronic and mechanical properties of TiPdSn.

2. Computational details

The density functional theory (DFT) is the basis behind the first principles calculation employed in this study. The exchange-correlation was taken care of by using the generalized gradient approximation and the projector augmented wave (PAW) type of pseudopotential as implemented in Quantum Espresso code was used[22]. Before any property is computed, it is important to optimise certain parameters which are responsible for achieving the lowest ground state energy of the compound. These parameters include the Kinetic energy cut-off, the kpoint and the lattice constants. The kinetic energy cut-off of 65Ry and a kpoint of 8X8X8 were used throughout the calculation with a convergence threshold of 10-6ev for better results. As for the lattice constant, the total energy versus the lattice constant graph was fitted to a Birch-Murnaghan equation of state in order to determine the optimised value. In order to take Brillouin zone samples, we used Monkhorst-Pack meshes with dimensions of 8x8x8 and 9x9x7, respectively, for the cubic and hexagonal half-Heusler alloys of TiPdSn. The Broyden-Fletcher-Goldfarb-Shenno (BFGS) minimization approach was used in order to carry out a comprehensive optimisation of the uniit cell structure for each individual target external pressure. This gives a quick method for locating the structure with the lowest energy and the cell that has been optimised at a variety of hydrostatic pressures. Mechanical and optical properties were computed using the Thermo_pw code [23]

3. Results and discussion

3.1 Structural properties

Half-Heusler alloys are known to cystallize in the face centered cubic structure having space group F-43m with no. 216. The crystal structure is shown in Fig. 1a. Other crystal structure that the half-Heusler alloys can crystallize is the hexagonal crystal structure with space group P63/mmc. There are two possible phases represened as type1 and type2 with their Wyckoff positions Ti at 2d (1/3, 2/3, 3/4), Pd at 2a (0, 0, 0) and Sn at 2c (1/3, 2/3, 1/4) for type 1 and Sn at 2d (1/3, 2/3, 3/4), Ti at 2a (0, 0, 0) Pd at 2c $(1/3, 2/3, \frac{1}{4})$ for type 2 as shown in Figs. 1b and c. The structural parameters of TiPdSn in the cubic phase, as well as in hexagonal phase for type1 and type2 are presented in Table 1. Results from this work are in good agreement with other results from literature [17,19]. A graph of the total energy vs the volume of the three phases are shown in Fig. 2. It is observed that the cubic phase is the most stable with the lowest ground state energy of the three phases. Structural phase transition is possible when materials are subjected to pressure [21]. The structural phase transition pressure of TiPdSn from cubic phase to type 1 and type 2 hexagonal phases are 25.3 Gpa and 4.53GPa respectively. These results can be clearly seen from Fig. 3. Table 2 shows the effect of pressure on the lattice constant of TiPdSn in

cubic phase as well as the bond length between two atoms. It is observed that these parameters dercrease as the pressure increases.

3.2 Electronic properties

The electronic property of TiPdSn has been investigated and are presented in this section in the form of electronic band structure and density of states (DOS) see Figs. 4 and 5. From the figures, it is seen that the half-Heusler alloy is a semiconductor with an indirect band gap of 0.465eV in the cubic phase at zero pressure while a metallic character is observed in the hexagonal type 2 phase at the transiton pressure of 4.53GPa. The contribution of each atomic orbital is seen in their corresponding DOS. Below the Fermi energy, there is a strong hybridization between the Ti orbital and the Sn orbital which shows a strong covalent bonding between the orbitals of these two atoms, while above the Fermi energy there is a weak covalent bonding between the Ti orbitals and the Sn orbitas for the cubic phase. In Fig. 5, it is observed that there is a metallic bonding between the Ti-d atomic orbitals and the Pd-d atomic orbitals around the Fermi energy. The behaviour of the band gap as pressure increases from 0-4.53GPa in shown in Table 2. It is øbserved that there is a very little increase in the band gap within the pressure range considered. At the transition pressure, it is observed that there is also a phase transition from semiconducting character to metallic character.

(1) C11 >0, C44 >0, C11 >B>C12 and C11+2C12 >0, C11-C12 >0

From the stability criteria, it is orbserved that TiPdSn is mechanically stable at zero pressure. At various pressures the stability criteria also holds. From the B/G ratio, it is observed that TiPdSn is ductile in nature. At higher pressures, the mechanical property of TiPdSn in cubic and Hex-2 have also been computed and are presented in Figs. 6-9. It is observed that the elastic constants increase as pressure increases likewise other parameters like the moduli, the B/G ratio and the poisson ratio increased with increasing pressure. At the transition point from cubic to hex-2, it is observed that there is a significant change in the mechanical behaviour of TiPdSn. This change is as a result of the phase transition from semiconducting character to mechanical character.

3.4 Optical Properties

The parameters associated with optical properties of TiPdSn are presented and discussed in this section. The optical property are plotted against energy in eV and are shown in Figs. 10 and 11. The optical properties are related to the dielectric functions $\varepsilon(\omega) = \varepsilon_1(\omega) + i\varepsilon_2(\omega)$ where $\varepsilon(\omega)$ is the amount of information regarding the interaction of incoming radiation with matter. $\varepsilon_1(\omega)$ and $\varepsilon_2(\omega)$ are the real and imaginary dielectric function. Optical properties such as the refractive index, reflectivity, absorption, energy loss, optical conductivity and extinction coefficient are determined from the real and imaginary dielectric function[24].

Table 1: Lattice parameter a and c, bulk modulus (B), and pressure derivative (B') of TiPdSn for cubic and hexagonal phases.

Compounds TiPdSn	Method	a(Å)	c(Å)	B(GPa)	В'
Cubic	Present work	6.222	-	118.7	4.62
	Others[17]	6.17	-	131.21	-
	Others[19]	6.23	-	-	-
Type 1	Present work	4.763	5.556	-	-
Type 2	Present work	4.628	5.796	-	-

Table 2: Lattice parameter a, bond length d_0 and d_1 and energy band gap E_g of TiPdSn at various pressure in cubic and hexagonal type 2 phase.

Compounds	Pressure	a(Å)	c(Å)	d ₀ (Å)	d ₁ (Å)	E _g (eV)
TiPdSn	(GPa)			Sn-Pd	Sn-Ti	
Cubic	0	6.222	-	1.556	3.111	0.4652
	2.00	6.141	-	1.537	3.075	0.4691
	4.42	6.075	-	1.519	3.038	0.4736
Hex-2	4.53	4.586	5.716	2.293	2.858	0.0000
	6.00	4.573	5.690	2.286	2.845	0.0000
	8.00	4.556	5.660	2.278	2.830	0.0000

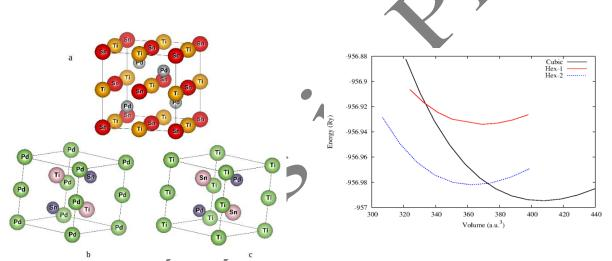


Figure 1: Crystal structure of TiPdSn alloys in (a) cubic phase, (b) hexagonal type 1 and (c) hexagonal type 2

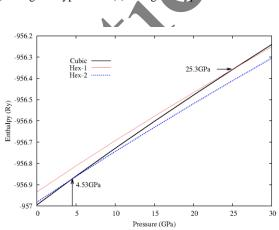


Figure 3: Enthalpy vs pressure of TiPdSn in the three phases.

Figure 2: Energy vs volume of TiPdSn for the three phases

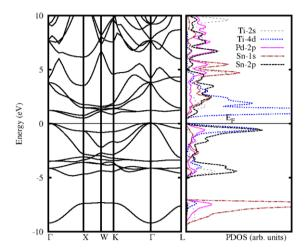


Figure 4: Electronic band structure and DOS of TiPdSn in cubic phase at zero pressure.

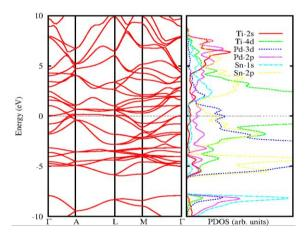


Figure 5: Electronic band structure and DOS of TiPdSn in hexagonal phase type 2 at 4.53GPa.

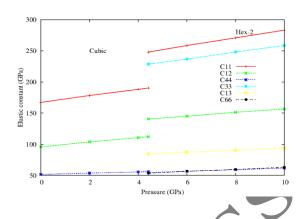


Figure 6: Elastic constants of TiPdSn in cubic and hexagonal type 2 phase.

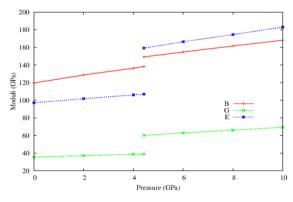


Figure 7: Bulk (B), Shear (G) and Young (E) moduli of TiPdSn in cubic and hexagonal type 2 phase.

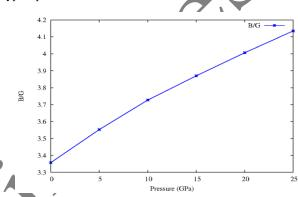


Figure 8: B/G ratio of TiPdSn in cubic phase.

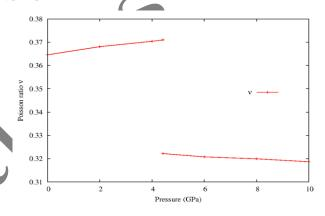


Figure 9: Poisson's ratio of TiPdSn in cubic and hexagonal type 2 phase.

Table 3: Mechanical properties of TiPdSn in cubic phase at zero ptrssure with C11, C12 and C44 as elastic constants, Young modulus E, shear modulus G, anisotropy A, B/G ratio and the Poisson's ratio v of TiPdSn. Results in parenthesis are from [17].

Compound	TiPdSn
$C_{II}(GPa)$	167.10(184.96)
$C_{12}(GPa)$	95.87(105.27)
$C_{44}(GPa)$	51.71(58.97)
E(GPa)	97.00(134.11)
G(GPa)	35.61
B/G	3.359
A	1.452
v	0.365(0.330)

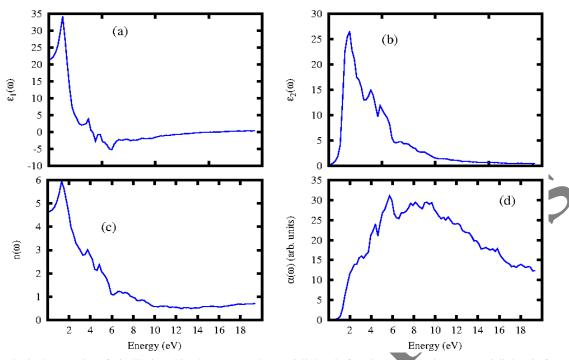


Figure 10: Optical properties of TiPdSn in cubic phase (a) Real part of dielectric function, (b) imaginary part of dielectric function, (c) Refractive index and (d) Absorption coefficient.

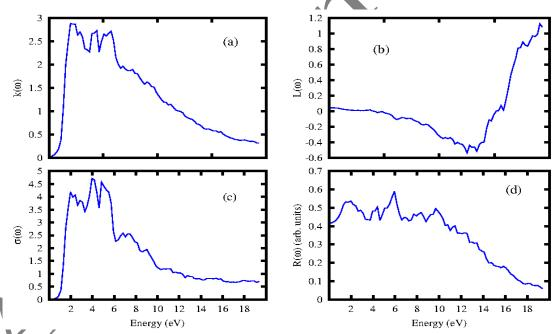


Figure 11: Optical properties of TiPdSn in cubic phase (a)Extinction coefficient, (b) Energy loss, (c) Optical conductivity and (d) Reflectivity.

Fig. 14a shows the real dielectric function of TiPdSn and it is orbserved that the static dielectric constant $\varepsilon_1(0)$ is 21.47 which is in good agreement with literature [13]. Fig. 10b shows the imaginary dielectric function having its highest peak at 1.97eV which falls within the visible light region of the spectrum. These peaks represent the various inter-band transition from the valence band to the conduction band. The refractive index of TiPdSn is shown in Fig. 10c and it is observed that the static refractive index is 4.63, Fig. 10d is the absorption coefficient which informs how light is absorbed by a material. It is observed

that the absorption coefficient gradually increases with increasing photon energy from about 0.56eV which corresponds to the energy band gap of TiPdSn. Above this energy, a sharp rise in the graph is observed indicating that TiPdSn absorbes a lot of light which in turn allows electrons to be excited to the conduction band region. The extinction coefficient of TiPdSn is shown in Figs. 11a which increases with increasing photon energy. It attains a maximum peak at 1.97eV with several other peaks occuring as the photon energy increases before gradually decreasing. During inelastic scattering of electrons with

light, energy is lost and this is described by Figs. 11b. From 13eV to 19eV, the energy loss is as a result of electron excitations. The optical conductivity of TiPdSn is shown in Figs. 11C with several peaks appearing within the energy range considered with the highest peak occuring at 3.96eV. The reflectivity is shown in Figs. 11d with the highest peak at 5.9eV revealing its maximum reflectivity of 59%. The maximum reflectivity within the visible light region is found to be 53%.

4. Conclusion

In summary, physical properties of TiPdSn have been investigated from first-principles calculation at zero and

at higher pressures. TiPdSn was found to be an indirect band gap semiconductor. Structural phase transition was observed from cubic phase to two different hexagonal phases. The mechanical properties reveal that the Half-Heusler alloys are ductile, with the elasric constants increasing with increasing pressure, also with the moduli increasing with increasing pressure and that the mechanical stablility was achieved. The optical properties of TiPdSn reveal that the half-Heusler alloy application in the opto-electronic industries.

calculation at zero and

References

- 1. Zilber, T., Cohen, S., Fuks, D. and Gelbstein, Y., 2019. TiNiSn half-Heusler crystals grown from metallic flux for thermoelectric applications. Journal of Alloys and Compounds, 781, pp.1132-1138.
- 2. Kocak, B. and Ciftci, Y.O., 2018. The effect of pressure on structural, electronic, elastic, vibration and optical properties of ScXSb (X= Ni, Pd, Pt) compounds. Computational Condensed Matter, 14, pp.176-185.
- 3. Babalola, M.I. and Iyorzor, B.E., 2019. A search for half metallicity in half Heusler alloys. Journal of Magnetism and Magnetic Materials, 491, p.165560.
- 4. Inomata, K., Okamura, S., Goto, R. and Tezuka, N., 2003. Large tunneling magnetoresistance at room temperature using a Heusler alloy with the B2 structure. Japanese journal of applied physics, 42(4B), p.L419.
- 5. Babalola, M.I. and Iyorzor, B.E., 2021. Electronic, mechanical, vibrational and optical properties of TaIrX (X= Ge and Sn): a DFT approach. Molecular Physics, p.e1995062.
- 6. Goll, G., Marz, M., Hamann, A., Tomanic, T., Grube, K., Yoshino, T. and Takabatake, T., 2008. Thermodynamic and transport properties of the non-centrosymmetric superconductor LaBiPt. Physica B: Condensed Matter, 403(5-9), pp.1065-1067.
- 7. Chadov, S., Qi, X., Kübler, J., Fecher, G.H., Felser, C. and Zhang, S.C., 2010. Tunable multifunctional topological insulators in ternary Heusler compounds. Nature materials, 9(7), pp.541-545.
- 8. Van Engen, P.G., Buschow, K.H.J., Jongebreur, R. and Erman, M., 1983. PtMnSb, a material with very high magneto-optical Kerr effect. Applied Physics Letters, 42(2), pp.202-204.
- 9. Babalola, M.I., Iyorzor, B.E. and Okocha, O.G., 2019. Origin of half-metallicity in XCrBi (X= Hf, Ti, and Zr) half-Heusler alloys. Materials Research Express, 6(12), p.126301.
- 10. Webster, P.J., Ziebeck, K.R.A., Town, S.L. and Peak, M.S., 1984. Magnetic order and phase transformation in Ni2MnGa. Philosophical Magazine B, 49(3), pp.295-310.
- 11. Canfield, P.C., Thompson, J.D., Beyermann, W.P., Lacerda, A., Hundley, M.F., Peterson, E., Fisk, Z. and Ott, H.R., 1991. Magnetism and heavy fermion-like behavior in the RBiPt series. Journal of applied physics, 70(10), pp.5800-5802.
- 12. Oogane, M., Sakuraba, Y., Nakata, J., Kubota, H., Ando, Y., Sakuma, A. and Miyazaki, T., 2006. Large tunnel magnetoresistance in magnetic tunnel junctions using Co2MnX (X= Al, Si) Heusler alloys. Journal of Physics D: Applied Physics, 39(5), p.834
- 13. Gautier, R., Zhang, X., Hu, L., Yu, L., Lin, Y., Sunde, T.O., Chon, D., Poeppelmeier, K.R. and Zunger, A., 2015. Prediction and accelerated laboratory discovery of previously unknown 18-electron ABX compounds. Nature chemistry, 7(4), pp.308-316.
- 14. Khandy, S.A. and Chai, J.D., 2021. Strain engineering of electronic structure, phonon, and thermoelectric properties of p-type half-Heusler semiconductor. Journal of Alloys and Compounds, 850, p.156615.
- 15. Damewood, L., Busemeyer, B., Shaughnessy, M., Fong, C.Y., Yang, L.H. and Felser, C., 2015. Stabilizing and increasing the magnetic moment of half-metals: The role of Li in half-Heusler LiMn Z (Z= N, P, Si). Physical Review B, 91(6), p.064409.
- 16. Kaur, K., 2017. TiPdSn: A half Heusler compound with high thermoelectric performance. EPL (Europhysics Letters), 117(4), p.47002.
- 17. Dasmahapatra, A., Daga, L.E., Karttunen, A.J., Maschio, L. and Casassa, S., 2020. Key Role of Defects in Thermoelectric Performance of TiMSn (M= Ni, Pd, and Pt) Half-Heusler Alloys. The Journal of Physical Chemistry C, 124(28), pp.14997-15006.
- 18. Zheng, W., Lu, Y., Li, Y., Wang, J., Hou, Z. and Shao, X., 2020. Structural and thermoelectric properties of Zr-doped TiPdSn half-Heusler compound by first-principles calculations. Chemical Physics Letters, 741, p.137055.
- 19. Gautier, R., Zhang, X., Hu, L., Yu, L., Lin, Y., Sunde, T.O., Chon, D., Poeppelmeier, K.R. and Zunger, A., 2015. Prediction and accelerated laboratory discovery of previously unknown 18-electron ABX compounds. Nature chemistry, 7(4), pp.308-316.
- 20. Noda, Y., Shimada, M. and Koizumi, M., 1979. Synthesis of high-pressure phases of vanadium-cobalt-antimony

- (VCoSb) and vanadium-iron-antimony (VFeSb) with a dinickel-indium (Ni2In)(B82) type structure. Inorganic Chemistry, 18(11), pp.3244-3246.
- 21. Gu, J.B., Wang, C.J., Cheng, Y., Zhang, L., Cai, L.C. and Ji, G.F., 2015. Structural, elastic, thermodynamic, electronic properties and phase transition in half-Heusler alloy NiVSb at high pressures. Computational Materials Science, 96, pp.72-80.
- 22. Giannozzi, P., Andreussi, O., Brumme, T., Bunau, O., Nardelli, M.B., Calandra, M., Car, R., Cavazzoni, C., Ceresoli, D., Cococcioni, M. and Colonna, N., 2017. Advanced capabilities for materials modelling with Quantum ESPRESSO. Journal of physics: Condensed matter, 29(46), p.465901.
- 23. Dal Corso, A. "Elastic constants of beryllium: a first-principles investigation." Journal of Physics: Condensed Matter 28, no. 7 (2016): 075401.
- 24. Sarker, S., Rahman, M.A. and Khatun, R., 2021. Study of structural, elastic, electronics, optical and thermodynamic properties of Hf2PbC under pressure by ab-initio method. Computational Condensed Matter, 26, p.e00512

